RELATIONSHIP BETWEEN SOLAR ENERGETIC PARTICLE HE/H ABUNDANCE RATIOS AND PROPERTIES OF FLARES AND CMES

THESIS

Christopher R. Davidson, Capt, USAF

AFIT-ENP-MS-21-S-025

DEPARTMENT OF THE AIR FORCE
AIR UNIVERSITY

AIR FORCE INSTITUTE OF TECHNOLOGY

Wright-Patterson Air Force Base, Ohio

AFIT-ENP-MS-21-S-025

RELATIONSHIP BETWEEN SOLAR ENERGETIC PARTICLE HE/H ABUNDANCE RATIOS AND PROPERTIES OF FLARES AND CMES

THESIS

Presented to the Faculty

Department of Engineering Physics

Graduate School of Engineering and Management

Air Force Institute of Technology

Air University

Air Education and Training Command

in Partial Fulfillment of the Requirements for the

Degree of Master of Science in Applied Physics

Christopher R. Davidson, B.S.

Capt, USAF

September 2021

AFIT-ENP-MS-21-S-025

RELATIONSHIP BETWEEN SOLAR ENERGETIC PARTICLE HE/H ABUNDANCE RATIOS AND PROPERTIES OF FLARES AND CMES

THESIS

Christopher R. Davidson, B.S.
Capt, USAF

Committee Membership:

Robert D. Loper, Ph.D.
Stephen W. Kahler, Ph.D.
Maj. Daniel J. Emmons, Ph.D.

AFIT-ENP-MS-21-S-025

Abstract

Previous studies have investigated the He/H elemental abundance ratios of Solar Energetic Particle (SEP) Events of energies above 4 MeV. Also, studies have investigated the correlations between SEPs, Coronal Mass Ejections (CME), and Solar Flares. This work finds the correlations between the >4 MeV He/H abundance ratios and the solar parameters from the SEP, CME, and solar flare associated with the abundance increases. 43 SEP events located at solar west longitude are analyzed to find the correlation coefficients. Highly significant correlation was found between the He/H abundance ratios and the following parameters: solar flare flux, solar flare fluence, CME linear speed, and SEP peak intensity. No correlation was found between the He/H abundance ratios and the following parameters: solar longitude, CME width, CME mass, and solar flare duration.

To my wife and daughter

Acknowledgements

Thank you to my family and my advisors for getting me through this difficult process. Many years of hard work have finally paid off.

Christopher R. Davidson

Table of Contents

Page

List of Figures

List of Tables

RELATIONSHIP BETWEEN SOLAR ENERGETIC PARTICLE HE/H ABUNDANCE RATIOS AND PROPERTIES OF FLARES AND CMES

I. Introduction

1.1 Motivation

The founding of the Unites States Space Force on December 20th, 2019 re-emphasized the United States acknowledgement that space is a warfighting domain. Joint Publication 3-14, Space Operations, identifies the space environment as a threat to space operations (DoD, 2018). One of the primary space environment threats is a Coronal Mass Ejection (CME) which produces a Solar Energetic Particle (SEP) event. During a CME, protons are ejected out of the Sun with energies exceeding 100 MeV and fluences that increase the chances of a satellite having an anomaly. The daily energetic proton fluences are predicted by the Space Weather Prediction Center (SWPC). During a SEP event the abundances of >10 MeV elements with Z>2 is also increased. No organization currently predicts the daily abundances of Z>2 atoms.

Already monitored by the SWPC are: proton abundances, sunspots, solar flares, and CMEs. If a correlation exists between the higher-Z relative abundance during a CME and any of the other solar phenomena already measured by the SWPC, two problems will be solved; the need for a separate sensor to detect higher-Z particles during an event will not be needed, and speed-of-light solar phenomena can give a warning to satellite operators before the greater abundance of higher-Z elements arrive in the near-Earth space environment.

Another reason to look for correlations between high-Z relative abundances during

SEP events is to help understand the mechanisms at the sun that generate these SEP events. Understanding why correlations exist between different solar phenomena will help to understand the solar mechanisms that produce the SEP events. Likewise, a better understanding of the solar CME process might lead to new and/or improved detection technics to give the satellite operators more information on the environment in which they operate.

1.2 Previous Work

Previous studies have delved into calculating the elemental abundances of elements heavier than Hydrogen during SEP events. Earlier studies have focused on the lower energy range abundances with energy ranged between 5-12 MeV/nucleon (Reames, 2018). The lower energy range provides a larger abundance value for study as well as access to study smaller SEP events due to still having statistically significant particle counts. Reames (2018) also focused on Oxygen and Iron as these elements have found to be the most relatively abundant elements during a SEP. Studies have also looked into the higher energy abundances. Hydrogen normalized relative abundance value for Helium, Carbon, Oxygen, Magnesium, and Iron were determined for the higher energy range of 13-50 MeV/nucleon (Round et al., 2016). Studies have also looked at examining how the SEP abundances vary with nucleon energy. Power-law fitting the elemental fluence when compared to the nucleon energy has been found to be an accurate model for use of abundance calculations (Desai et al., 2016). Desai's power-law calculation have focused on the Hydrogen, Oxygen, and Iron due to their higher relative abundances. Previous studies have also attempted to analyze if the mass-to-charge ratio play any impact of the SEP abundances (Reames, 2020). Similar to other studies, Reames (2020) focused on Hydrogen, Helium, Oxygen, and Iron.

Multiple studies comparing SEP events to other solar parameters have been ac-

complished. A statistical analysis of solar cycle 23 found correlation coefficients (CC) between >10MeV protons and both flare intensity and CME speed (Dierckxsens et al., 2015) of 0.55 ± 0.07 and 0.56 ± 0.08, respectively. In Dierckxsen's study, no correlation was found between the energetic protons and neither flare longitude nor CME width. A strong correlation between peak intensities of deka-MeV protons with the maximum microwave fluence, the projected CME speed, and start-to-peak soft X-ray (SXR) fluence with correlation ranges between 0.61 and 0.76 (Trottet et al., 2015). Significant correlation exists between suprathermal particles and SEP event peak intensity from solar longitude of 0° to W40° (Kahler and Ling, 2019). SEP He/H peak intensity ratios (A_{He}) in the 21–41 and 41–53 MeV/nuc range correlated to the solar wind (SW) A_{He} with CC of 0.42 and 0.41, respectively (Kahler and Brown, 2021). This work will focus on identifying correlations between SEP He/H peak intensity ratios and the five associated solar parameters: X-ray flare source solar longitude, peak SXR flux of the flare, duration of the X-ray flare, speed of the CME, and width of the CME.

1.3 Problem Statement

He/H relative abundances in the solar wind change among different SEP events. Does a correlation exist between the relative He/H abundances and the following solar parameters: flare solar longitude, flare flux, duration of the solar flare, linear speed of the associated CME, mass of the CME, kinetic energy of the CME, acceleration of the CME, angular width of the CME, and SEP peak intensity? If so, measuring one of the parameters can give satellite operators a warning of the increase in higher-Z elements before they reach near-Earth.

II. Background

2.1 Solar Wind

The Sun is the primary producer of radiation in the inner solar system. Forming from the Corona, the solar wind is a stream of plasma that emanates radially from the Sun. This solar wind radiates out through the planets into the interstellar medium accelerating from the corona. Parker found a transcendental equation to find the solar wind velocity and a function of the plasma isothermal sound speed (Parker, 1958). As the distance to the sun increases, the speed of the solar wind increases. By measuring the solar wind speed at earth, the Parker model can give a good estimate of coronal temperature.

The solar wind consists of 91-95% protons, 4-8% helium, and the rest consists of higher-Z elements (Pisacane, 2008). There are an equal number of electrons in the solar wind to make the solar wind electrically neutral.

Due to a misalignment between the Sun's magnetic rotation axis, the Sun's polar rotation axis, the Earth's magnetic rotation axis, and the Earth's polar rotation axis, the solar wind creates a Heliospheric current sheet and arrives in a ballerina skirt shape (Parker, 1958).

From the axes mismatches, the solar wind arrives at angles that vary between 45 and 225 degrees of Earth's polar rotation axis. In instances where a faster solar wind approaches and meets a slower solar wind, the angle at which it arrives will abruptly change.

The plasma speeds of the solar wind are not constant and can vary between 300 and 800 km/s. At these speeds, the solar wind protons have energies of 1-2 keV. Due to the different speeds, the densities of the solar wind can vary between 3 and 10 particles cm^{-3}.

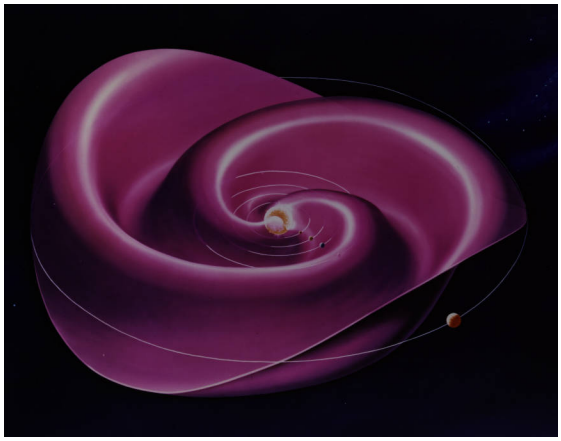

Figure 1. Heliospheric Current Sheet (Zell, 2015)

This variation produces a proton flux density of $1.2 - 5 \times 10^{12}\ m^{-2}s^{-1}$ protons that are colliding with the Earth's Magnetosphere (Pisacane, 2008). A small fraction of the solar wind flux is made of elements heavier than Helium.

2.2 Sunspots

The Sun is not a uniform celestial body. The hot plasma that makes up the Sun's photosphere cannot maintain a dipole, dissimilar to the one Earth maintains. Unlike the Earth, different latitudes of the Sun rotate at different angular velocities. The rotation varies from as fast as 25 days at the equator to 35 days at the poles. This varying solar rotation is one theory as to the generation of Sun's magnetic field. As the rotations progress, the Sun's magnetic field begins to twist and contort. As the contortion continues, the Sun loses its dipole shape. Some magnetic field lines, not near the magnetic poles, become open field lines. Some closed loop fields shrink in size. Figure 3 shows the magnetic field lines during solar minimum and maximum.

Often, a concentration of magnetic field lines will emerge from one section on the Sun and loop to another section on the sun. If the concentration of field lines is sufficient, a sunspot pair may form. /par

A sunspot is a cooled section of the photosphere when compared to the surround-

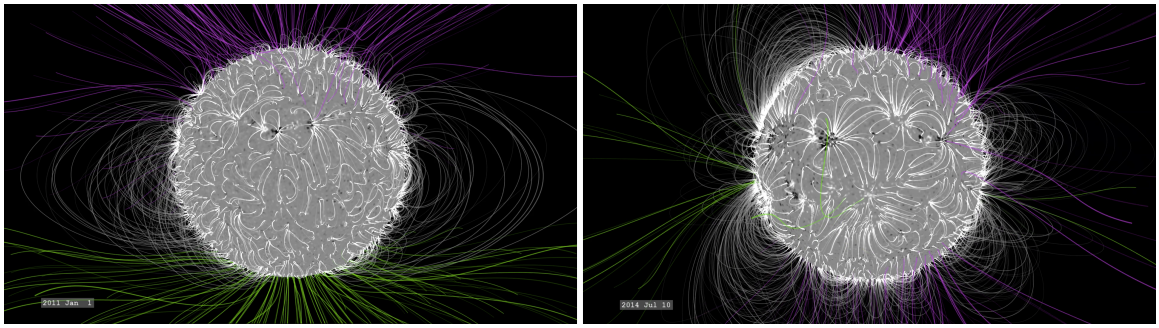

Figure 2. Solar magnetic field during solar minimum (left) and solar maximum (right). (Frazier, 2016)

ing photosphere. While the normal photosphere has a temperature of 5,800 K, the photosphere temperature drops to 3,800 K. This 2,000 K temperature drop lowers the radiance due to black-body radiation by a factor of 5, giving the sunspot a relatively dimmer appearance than the surrounding photosphere.

2.3 Solar Flares

A solar flare consists of large eruptions of electromagnetic activity from the Sun. These eruptions from the Sun can last anywhere from minutes to hours. Solar flares emit radiation, plasma, particles, and radio waves into space.

Magnetic field lines of the Sun can become twisted and contorted. This twisting and contortion usually occurs near sunspots. The leading theory behind the cause of solar flares is that they are caused by magnetic reconnection on the surface of the sun. They are usually found near groups of Sunspots and occur over active regions of electromagnetic activity. Active regions are regions of the Sun exhibiting strong magnetic fields at the same location as sunspot groups. Because of this link to sunspots, the more sunspots the Sun has, the more solar flares that will exist.

Solar flares are not surface level events on the Sun. They extend further into the solar atmosphere than the surface and affect the photosphere, chromosphere, and corona. This expels electromagnetic radiation across all wavelengths of the electro-

magnetic spectrum. Since most wavelengths are not visible to the naked eye, most solar flares are also not visible and must be observed using special instruments.

Of the many wavelengths emitted by solar flares, it is of importance to note 10.7 cm radio emissions. The F10.7 index, as it is often called, is currently considered one of the longest running records of solar activity. As previously mentioned, because solar flares exist throughout all levels of the sun's atmosphere, the F10.7 emissions extend from high in the chromosphere down through the lower in the corona. The number of sunspots correlates with the F10.7 as well and there is an noticeable correlation to the measurements of UV (Ultraviolet) and visible solar irradiance records. The F10.7 is one of the few emissions that can be measured on a day to day basis from the surface of the Earth.

There are 5 classifications of solar flares: A, B, C, M, and X. Each classification is measured in peak flux in watts per square meter of X-rays with wavelengths 100-800 picometres. The class of a flare is then noted with a numerical suffix from 0-9. The numerical suffix is the factor for an event within that class.

Classification	Peak Flux (W m^{-2})
A	$< 10^{-7}$
B	$10^{-7} - 10^{-6}$
C	$10^{-6} - 10^{-5}$
M	$10^{-5} - 10^{-4}$
X	$< 10^{-4}$

Table 1. Solar Flare Classifications

The largest solar flare on record was observed by the ESA-NASA SOHO spacecraft on Monday 4 November 2003. The flare saturated the GOES X-ray detector for 12 minutes. The detector of GOES-12 saturates at a X17.4 flare. It has been classified as an X23.0 (Brodrick et al., 2005).

2.4 Coronal Mass Ejections

Large emissions of plasma and magnetic field from the corona of the Sun are called Coronal Mass Ejections (CME). CMEs often occur in tandem with solar flares. A single CME can eject billions of tons of material from the corona and carry a strong magnetic field. Plasma from a CME is released into the solar wind. When the sun is near Solar Maxima, it can release approximately three CME/s every day. Conversely, when the sun is near Solar Minima, only one CME is released approximately every five days.

CMEs travel outwards from the sun at speeds as fast as 3,000 km/s or slower than 250 km/s. Faster traveling CMEs may reach the Earth's atmosphere in as little as 15-18 hours, but slower ones may take as many as several days to reach Earth. In some instances, CME's occasionally travel faster than the background solar wind. When this happens, a shock wave may be generated. Shock waves may also accelerate particles ahead of them and as a result increase the potential or intensity of a radiation storm. Important parameters to keep in mind when discussing CMEs are size, speed, and direction.

In much the same way that solar flares are believed to be caused by magnetic reconnection, CMEs share that phenomenon. One theory, the magnetohydrodynamic theory (MHD), explains magnetic reconnection as two oppositely directed magnetic fields being brought together. The result of this coming together of magnetic fields is a release of energy that was originally stored in the stressed magnetic fields. Twisted magnetic fields form a helical structure and as they twist CMEs release the pent up energy.

On 1-2 September 1859, during solar cycle 10, a CME that hit Earth's magnetosphere caused the largest geomagnetic storm on record. This event was labeled as The Carrington Event. The CME took 17.6 hours to reach Earth after ejection from

the Sun. Auroras were seen around the world and telegraph systems all over North America and Europe failed.

2.5 SEP events

Observed first in the 1940's, Solar energetic particles (SEP) are high energy particles that come from the sun. These particles can range from protons, electrons, and high atomic number and energy (HZE) ions and have energy fluctuations ranging from tens of keV to GeV. Solar energetic particles are ejected from solar flares and coronal mass ejections (CME). While SEP event accelerations can be within a large range of speeds, most can be classified into two specific categories of SEP events: impulsive and gradual.

2.6 Impulsive SEP events

Short solar energetic particle events with a duration of only a few hours, Impulsive SEP events, are characterized as "pure" electron events and are associated primarily with Type III radio bursts. When magnetic reconnection causes acceleration of electron beams that are accelerated in small proportions of the speed of light (around 0.1 to 0.3c), Type III radio bursts occur. Type III radio bursts are strongly associated with solar flares producing x-ray wavelengths and are observed in most large solar flares. In addition, Impulsive SEPs have low peak intensities and originate from CME events that are narrow and slow and originating in solar jets. Impulsive SEP events are often called ^{3}He-rich events due to the abundance of the isotope ^{3}He where ^{3}He can be increased by a factor of up to 10^4. That said, it has been concluded that Fe abundance is a greater indication of impulsive events than ^{3}He due to the stronger reliability of its energy strength (Reames, 2018). Further, the acceleration of electrons within an impulsive SEP was found to generate electromagnetic ion cyclotron

(EMIC) waves that would create a magnetic mirror and accelerate ^{3}He ions. Impulsive SEP events have also been found to have a higher Z/O concentrations when compared to the corona for heavier ions such as Mg. The rate of production of ions can be explained by Equation 1 (Drake et al., 2009). The time rate of change of ions (dN/dt) is proportional to a mass (A) to charge (A) power law (α).

$$\frac{dN_i}{dt} \propto w^{3-\alpha} \propto \left(\frac{A}{Q}\right)^{\alpha-3}. \tag{1}$$

In addition, it is important to note that Impulsive SEP events rarely drive a shockwave due to the lack of Type II radio bursts and their narrower mean width (<75 degrees). (Reames, 2018).

2.7 Gradual SEP events

Gradual SEP events occur over much larger time scales (days) than Impulsive SEP events and are associated with Type II radio bursts. Type II radio bursts are associated with Coronal Mass Ejection (CME) and occur alongside shockwaves moving away from the sun. The longer time scale of gradual SEP events contributes to the event having a larger longitudinal spread of elevated energetic particles. Gradual SEPs are also associated with fast and wide Coronal Mass Ejections (CME) and have been known to produce ions with energies in the GeV range. A shock is produced in the plasma during Gradual SEP events and is the main contributor to the large energy gains of the ions including those remaining from previous impulsive SEP events. This can cause some confusion between the impulsive and gradual SEP types as these ions from previous impulsive events accelerate ahead of the shockwave associated with a gradual SEP event. The concentrations of high-Z ions compared to the Corona during a gradual SEP is altered. Gains and losses of high-Z concentrations have been noted among different CMEs that result in SEP event (Reames, 2016).

2.8 Elemental Abundances

The most common noted elemental abundances in the solar wind include C, N, O, Ne, Mg, Si, S, and Fe. Particles originating from the solar wind are able to escape the gravity of the sun primarily due to the high temperature of the corona providing additional energy to those ions. At a speed of $1.3x10^{36}$ per second, particles escape the sun at the rate of approximately 1.3-1.9 million tons per second. The solar wind is only capable of collecting ions escaping from the sun along open field lines.

During SEP events, the levels of P, S, and C are low while the levels of N are higher. Ions that eventually become SEPs originate with closed magnetic loops where concentrations are higher near the top of the chromosphere. Ions that begin on open field lines are more likely to become solar wind particles. It is important to note that the corona is fixed to the sun only by high closed magnetic loops which contain the plasma. Forceful CME shockwaves can break through those loops driving ions to MeV-energy SEPs causing them to escape the confines of the sun's corona. The largest difference in ion abundances between an SEP event and solar wind lies in the transition between high First Ionization Potential (FIP) and low-FIP elements. P, S, and C have been evidenced to be high-FIP elements during SEP events, but low-FIP elements for the solar wind. FIP is the amount of energy required to remove the most loosely held electron from a neutral atom.

Differences in open and closed field lines in the chromosphere may explain the differences in P and S abundances. These differences combined with a variation in the C/O between solar wind and SEPs cause the C, P, and S to behave as neutral atoms in SEP events, but as ions in the solar wind. In addition, while nuclear reactions in solar flares create detectable elemental abundances, the lack of ^{2}H, ^{3}H, Li, Be, and B in SEP events indicates that these events are not the result of escaping nuclear reactions of solar flares.

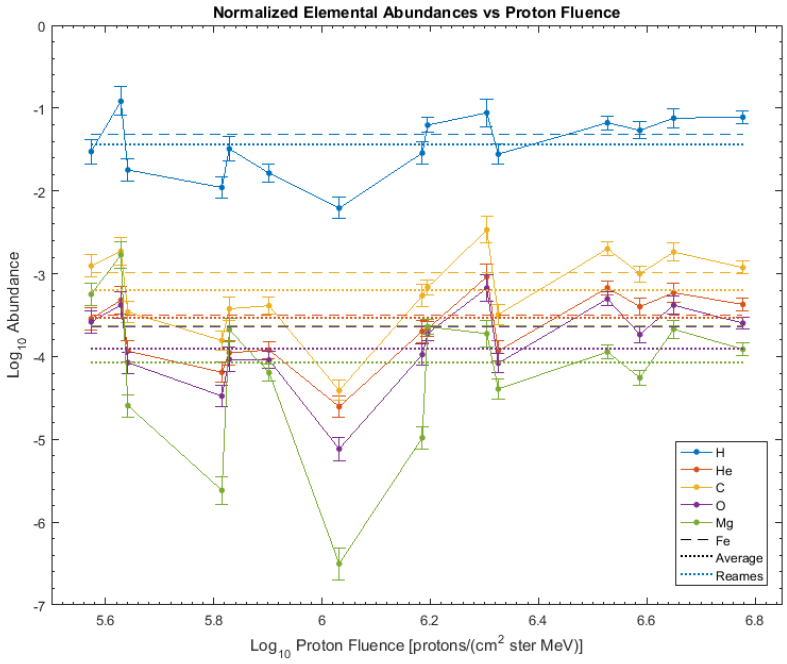

Figure 3. Normalized Elemental Abundance vs Proton Fluence. (Round, 2019)

III. Methodology

3.1 Defining Scope

The objective of this study was to determine if a correlation exists between the relative He/H (h/p) abundances and the following solar parameters: solar flare solar longitude, solar flare flux, solar flare duration, solar flare fluence, mass of the CME, kinetic energy of the CME, speed of the associated CME, and angular width of the CME, I_p. If we can find any existing correlation coefficients between these particle events, further studies may be able to explore causations of h/p abundance increases. With numerous solar events occurring each solar cycle and numerous sensors on orbit, the number of events and data sources had to be constricted for feasibility of project execution.

3.2 Solar Flare Locations

Due to the propagation and spread of the solar wind, data points for solar flare locations were selected from the Western hemisphere of the sun such that sensors on and near Earth could obtain accurate measurement of h/p particles. Table 4, provided by Kahler & Brown (2021), contains 43 data points that were considered relevant to the study of h/p particle abundances (Kahler and Brown, 2021).

3.3 Sensor and Data Selection

Used in this study are the various sensors at the Solar and Heliospheric Observatory (SOHO) and the Electron Proton Helium Instrument (EPHIN) located aboard SOHO. Data from the sensors aboard the SOHO was extracted from two separate sources: The SOHO LASCO CME Catalog compiled by the Coordinated Data Anal-

ysis Workshop (CDAWS) and the Solar Eruptive Event Detection System (SEEDS) compiled by the George Mason University Space Weather Lab.

Contained in the CDAWS charts is data about CME speeds, accelerations, mass, and kinetic energy. The CDAWS data reports CME speeds of 3 types: linear speed obtained by fitting a straight line to the height time measurements, quadratic speed obtained by fitting a parabola to the height time measurements and evaluating the speed at the time of final height measurement, and quadratic speed but evaluated when the CME is at a height of 20 solar radii. For the purposes of this study, we focused on the linear speed of CMEs. For the purposes of reporting accelerations of CMEs, the CDAWS requires a minimum of three height-time measurements, but more measurements provides more accurate acceleration reports. Mass measurements of CME as reported by the CDAWS data is taken at the point after which they transverse the first solar radii when mass reaches a near constant value. In instances where the CME fades before reaching the first solar radii, the CDAWS reports the mass at the last measurement. Kinetic energy is determined from linear speed and kinetic energy and reported on the data table. Finally, CDAWS reports data on the position angle at which the height-time measurement is made providing the CME width used in this study.

For the purposes of cross referencing data points, data extracted from the CDAWS computations was compared to the SEEDS data catalog. The SEEDS data catalog reports speed, acceleration, and position angle (width) of CMEs. Because SEEDS is a digital detection algorithm, it process through three stages of identification: pre-processing, detection, and tracking. Using these processes, SEEDS is able to track data related to the movement of CMEs. When used congruently, the SEEDS data catalog and the CDAWS catalog recover data from approximately 75% of CMEs that occur.

The EPHIN sensor measures solar energetic electrons, protons, and alpha particles. It consists of a stack of six solid state detectors that together form a telescope. EPHIN measures electrons from 250 keV to greater than 8.7 MeV and protons and He from 4 to 53 MeV nuc^{-}1 meeting our criteria for study.

The final sensors used in this study were the Energetic and Relativistic Nuclei and Electron (ERNE) experiment on SOHO. These sensors provided He and H numbers for comparison during the study of CME and SEP events being studied.

3.4 Time Period Selection

The time periods selected for study were limited to data points in which all necessary data was available for the necessary comparison. Because the study used data points from Kahler & Brown (2021), the time periods covered range from May 1998-September 2017. Data from CDAWS and SEEDS were available during these time periods as well and able to be used for comparison.

3.5 Elemental Selection

In order to keep the research constrained, the number of elements analyzed in this study was reduced to only He and H. Data from SOHO/ERNE was used to compile the quantities of He and H at the time of CMEs and solar flares.

3.6 Event Selection Criteria

For the purposes of this study, gradual SEP events were chosen as the focus due to their longer duration and higher element abundances. The focus was on SEP events that coincide with solar flares and resulted in CME. It was necessary to disregard any events in which multiple solar flares, CMEs, or SEP events occurred simultaneously.

3.7 Data Analysis Method

All solar parameters from CDAWS, SEEDS, ERNE, and Kahler & Brown (2021) being correlated was compiled. The data for the 43 SEP events from Kahler & Brown was then imported into MATLAB for finding of the Correlation Coefficient (CC). Equation 2, the Pearson Correlation Coefficient formula was used to ascertain correlations between the solar parameters in this study (Taylor, 1997). The Pearson Correlation is the ratio of the covariance between two variables and the product of their standard deviations. In equation 2 r is the CC aimed for in this study, while x_i and y_i are the data points of the two variables being correlated. It is of note that an equal number of data points is required for the equation. The CC will return a r-value between -1 and 1. A r=+1 is a perfect positive linear correlation. A r=-1 is a perfect negative linear correlation. A r=0 determines the two variable are unrelated.

$$r = \frac{\sum(x_i - \bar{x})(y_i - \bar{y})}{\sqrt{\sum(x_i - \bar{x})^2 \sum(y_i - \bar{y})^2}}. \tag{2}$$

As will all scientific and statistical calculation, error is induced. Equation 3 is the error of Pearson's Correlation Coefficient (Eells, 1929). The formula takes into account the r value from Equation 2 and the number of data points (N). CC error is reduced with a larger r value, and a larger number of data points.

$$\frac{0.6745(1 - r^2)}{\sqrt{N}}. \tag{3}$$

Data is rarely perfectly correlated. A $|r|$between 0 and 1 mean the data could potentially be correlated. An interpretation methodology is needed to give weight to the CC r-values. Equation 4 is a method to give confidence to an r-value and the two variable being correlated (Taylor, 1997). $Prob_N\left(|r| \geq |r_0|\right)$ is the probability that two uncorrelated variables return a r-value greater than the one found in 2 (r_0) with

a number of data points (N). Essentially, the probability of a false correlation being determined. Table 2 lists the r-values for the various N values used in this study to meet the 5% and 1% probability of giving false correlation criteria.

$$Prob_N\left(|r| \geq |r_0|\right) = \frac{2\Gamma[\frac{N-1}{2}]}{\sqrt{\pi}\,\Gamma[\frac{N-2}{2}]} \int_{|r_0|}^{1} (1-r^2)^{\frac{N-4}{2}} dr. \tag{4}$$

N	$Prob_N < 0.05$	$Prob_N < 0.01$
33	0.34	0.44
34	0.34	0.44
35	0.33	0.43
36	0.33	0.42
37	0.33	0.42
38	0.32	0.41
39	0.32	0.41
40	0.31	0.4
41	0.31	0.4
42	0.3	0.39
43	0.3	0.38

Table 2. Correlation Coefficient values for significant and highly significant correlation for various N's

IV. Analysis and Results

4.1 Event Selection

The SEP events selected by Kahler & Brown as show from Table 4 in were used as the starting point for this study (Kahler and Brown, 2021). The data utilized in that table are the start and stop times of the SEP. Using those times, the associated solar flare and CME for each SEP was found using the SEEDS and CDAW databases. Also utilized from Table 4 are the 4, 8 ,and 25 MeV h/p ratios, the solar wind (SW) h/p rations, and the peak SEP intensity.

Table 5 shows the selected solar flare and CME for each SEP used in this study. For each solar flare and CME selected, the following parameters from the CDAW and SEEDS databases were included in this correlation study: Solar Longitude, CME width, CME linear speed, CME kinetic energy, CME acceleration, CME Mass, solar flare peak proton flux, solar flare fluence, and solar flare duration. Tables 6 & 8 show the CME and solar flare parameters selected from the databases.

Year/Month	Day/Onset	Longitude	SEP I_p	h4/p4	h8/p8	h25/p25
1998 May	2/1400	W15	150	0.011	0.014	0.007
1998 May	6/0800	W65	210	0.055	0.024	0.002
1998 Nov	14/0600	W120	310	0.013	0.029	0.021
1999 Jun	1/2000	NW	48	0.006	0.009	0.005
2000 Jun	10/1700	W38	46	0.007	0.007	0.003
2000 Sep	12/1300	W09	320	0.012	0.008	N A
2001 Jan	28/1700	W59	25	0.004	0.006	0.002
2001 Apr	02/2200	W72	800	0.087	0.059	0.032
2001 Apr	15/1400	W85	951	0.028	0.018	0.030
2001 Aug	16/0100	SWL	493	0.018	0.016	0.012
2001 Oct	1/1200	W95	700	0.039	0.028	0.011
2001 Dec	26/0600	W54	779	0.023	0.017	0.002
2002 Apr	21/0200	W84	350	0.038	0.029	0.030
2002 Aug	22/0200	W62	36	0.009	0.010	0.004
2002 Aug	24/0100	W81	250	0.019	0.015	0.004
2003 Oct	26/1800	W38	466	0.044	0.024	0.012
2003 Nov	2/1800	W56	1570	0.063	0.037	0.026
2003 Nov	4/2000	W83	353	0.047	0.033	0.012
2004 Sep	19/1800	W58	40	0.007	0.005	0.001
2004 Nov	7/1800	W17	495	0.040	0.032	0.025
2004 Nov	10/0300	W49	300	0.045	0.039	0.010
2005 Jan	17/1000	W25	5040	0.040	0.043	0.046
2005 Jan	20/0700	W61	1100	0.067	0.048	0.063
2005 Jun	16/2100	W90	44	0.006	0.008	0.002
2005 Jul	14/1200	W90	110	0.048	0.042	0.015
2006 Dec	13/0200	W22	698	0.045	0.036	0.027
2006 Dec	14/2200	W46	160	0.004	0.006	0.002
2010 Aug	14/1000	W56	14	0.001	0.001	0.000
2011 Jun	7/0700	W53	50	0.007	0.010	0.005
2011 Aug	4/0500	W38	80	0.019	0.021	0.011
2011 Aug	9/0800	W69	26	0.020	0.023	0.011
2012 Jan	23/0400	W21	3500	0.041	0.024	0.023
2012 Jan	27/1900	W85	796	0.042	0.024	0.022
2012 Mar	13/1800	W66	469	0.009	0.009	0.004
2012 May	17/0200	W88	255	0.011	0.012	0.001
2012 Jul	19/0700	W88	75	0.016	0.020	0.011
2013 May	22/1400	W87	1660	0.012	0.011	0.006
2013 Sep	30/0000	W33	182	0.009	0.007	0.003
2014 Jan	7/1900	W11	900	0.024	0.013	0.007
2014 Apr	18/1400	W34	58	0.018	0.022	0.009
2015 Oct	29/0500	bWL	20	0.002	0.003	0.001
2017 Sep	6/1300	W46	50	0.005	0.008	0.032
2017 Sep	10/1600	W90	1200	0.034	0.027	0.018

Table 3. Kahler & Brown 2021 Data

Year/Month	Day/Onset	Longitude	SEP I_p	h4/p4	h8/p8	h25/p25
1998 May	2/1400	W15	150	0.011	0.014	0.007
1998 May	6/0800	W65	210	0.055	0.024	0.002
1998 Nov	14/0600	W120	310	0.013	0.029	0.021
1999 Jun	1/2000	NW	48	0.006	0.009	0.005
2000 Jun	10/1700	W38	46	0.007	0.007	0.003
2000 Sep	12/1300	W09	320	0.012	0.008	N A
2001 Jan	28/1700	W59	25	0.004	0.006	0.002
2001 Apr	02/2200	W72	800	0.087	0.059	0.032
2001 Apr	15/1400	W85	951	0.028	0.018	0.030
2001 Aug	16/0100	SWL	493	0.018	0.016	0.012
2001 Oct	1/1200	W95	700	0.039	0.028	0.011
2001 Dec	26/0600	W54	779	0.023	0.017	0.002
2002 Apr	21/0200	W84	350	0.038	0.029	0.030
2002 Aug	22/0200	W62	36	0.009	0.010	0.004
2002 Aug	24/0100	W81	250	0.019	0.015	0.004
2003 Oct	26/1800	W38	466	0.044	0.024	0.012
2003 Nov	2/1800	W56	1570	0.063	0.037	0.026
2003 Nov	4/2000	W83	353	0.047	0.033	0.012
2004 Sep	19/1800	W58	40	0.007	0.005	0.001
2004 Nov	7/1800	W17	495	0.040	0.032	0.025
2004 Nov	10/0300	W49	300	0.045	0.039	0.010
2005 Jan	17/1000	W25	5040	0.040	0.043	0.046
2005 Jan	20/0700	W61	1100	0.067	0.048	0.063
2005 Jun	16/2100	W90	44	0.006	0.008	0.002
2005 Jul	14/1200	W90	110	0.048	0.042	0.015
2006 Dec	13/0200	W22	698	0.045	0.036	0.027
2006 Dec	14/2200	W46	160	0.004	0.006	0.002
2010 Aug	14/1000	W56	14	0.001	0.001	0.000
2011 Jun	7/0700	W53	50	0.007	0.010	0.005
2011 Aug	4/0500	W38	80	0.019	0.021	0.011
2011 Aug	9/0800	W69	26	0.020	0.023	0.011
2012 Jan	23/0400	W21	3500	0.041	0.024	0.023
2012 Jan	27/1900	W85	796	0.042	0.024	0.022
2012 Mar	13/1800	W66	469	0.009	0.009	0.004
2012 May	17/0200	W88	255	0.011	0.012	0.001
2012 Jul	19/0700	W88	75	0.016	0.020	0.011
2013 May	22/1400	W87	1660	0.012	0.011	0.006
2013 Sep	30/0000	W33	182	0.009	0.007	0.003
2014 Jan	7/1900	W11	900	0.024	0.013	0.007
2014 Apr	18/1400	W34	58	0.018	0.022	0.009
2015 Oct	29/0500	bWL	20	0.002	0.003	0.001
2017 Sep	6/1300	W46	50	0.005	0.008	0.032
2017 Sep	10/1600	W90	1200	0.034	0.027	0.018

Table 4. Kahler & Brown 2021 Data

Year/Month	Day/Onset	GOES peak xray time	CDAW CME
1998 May	2/1400	13:41	14:06
1998 May	6/0800	8:08	8:29
1998 Nov	14/0600	5:18	NA
1999 Jun	01/2000	18:59	19:37
2000 Jun	10/1700	16:58	17:08
2000 Sep	12/1300	11:55	11:54
2001 Jan	28/1700	15:55	15:54
2001 Apr	02/2200	21:48	22:06
2001 Apr	15/1400	13:48	14:06
2001 Aug	16/0100	0:14	23:54
2001 Oct	1/1200	5:13	5:30
2001 Dec	26/0600	5:31	5:30
2002 Apr	21/0200	1:39	1:27
2002 Aug	22/0200	1:55	2:06
2002 Aug	24/0100	1:06	1:27
2003 Oct	26/1800	18:03	17:54
2003 Nov	2/1800	17:23	17:30
2003 Nov	4/2000	19:43	19:54
2004 Sep	19/1800	17:06	NA
2004 Nov	7/1800	16:05	16:54
2004 Nov	10/0300	2:11	2:26
2005 Jan	17/1000	9:49	9:30
2005 Jan	20/0700	6:56	6:54
2005 Jun	16/2100	20:17	NA
2005 Jul	14/1200	10:51	10:54
2006 Dec	13/0200	2:37	2:54
2006 Dec	14/2200	22:12	22:30
2010 Aug	14/1000	10:01	10:12
2011 Jun	7/0700	6:39	6:49
2011 Aug	4/0500	3:55	4:12
2011 Aug	9/0800	8:04	8:12
2012 Jan	23/0400	3:54	4:00
2012 Jan	27/1900	18:31	18:27
2012 Mar	13/1800	17:32	17:36
2012 May	17/0200	1:43	1:48
2012 Jul	19/0700	5:53	5:24
2013 May	22/1400	13:26	13:25
2013 Sep	30/0000	23:32	22:12
2014 Jan	7/1900	18:25	18:24
2014 Apr	18/1400	12:58	13:25
2015 Oct	29/0500	4:38	2:36
2017 Sep	6/1300	12:01	12:24
2017 Sep	10/1600	16:03	16:00

Table 5. SEP, Flare, and CME event times

CDAW Width	SEEDS Width	CDAW Speed	SEEDS Speed
360	91	938	745
190	131	1099	500
NA	NA	NA	NA
360	95	1772	105
360	35	1108	190
360	140	1550	252
360	173	916	196
244	95	2505	614
167	176	1199	202
360	266	1575	428
360	63	1405	96
212	105	1446	71
360	186	2393	703
360	88	998	770
360	186	1913	561
171	178	1537	312
360	171	2598	1053
360	135	2657	170
NA	16	NA	115
360	159	1759	150
360	61	3387	421
360	114	2094	612
360	52	882	125
NA	NA	NA	NA
360	85	2115	930
360	127	1774	786
360	115	1042	579
360	117	1205	657
360	120	1255	441
360	156	1315	384
360	62	1610	495
360	183	2175	700
360	272	2508	325
360	130	1884	378
360	115	1582	502
360	122	1631	865
360	150	1466	639
360	158	1179	441
360	197	1830	673
360	144	1203	171
202	26	530	190
360	145	1571	505
360	155	3163	921

Table 6. CME Speeds and Widths

CME KE	CME Accel	CME Mass
3.40E+31	-28.8	7.70E+15
1.80E+32	24.5	3.00E+16
NA	NA	NA
1.70E+32	1.8	1.10E+16
1.00E+32	-21.2	1.70E+16
2.60E+32	58.2	2.20E+16
5.00E+31	3.5	1.20E+16
2.90E+32	108.5	9.20E+15
5.90E+32	-35.9	8.20E+16
1.30E+32	-31.7	1.00E+16
NA	65.1	NA
5.00E+31	-39.9	4.80E+15
NA	-1.4	NA
NA	-32.8	NA
NA	43.7	NA
2.40E+32	4.8	2.00E+16
1.70E+32	-32.4	4.90E+15
1.80E+30	-146.2	3.40E+15
NA	NA	NA
2.20E+32	-19.7	1.40E+16
5.50E+32	-108	9.50E+15
NA	-159.1	NA
NA	16	NA
NA	NA	NA
1.10E+32	198	5.00E+15
7.40E+31	-61.4	4.70E+15
4.10E+31	-0.4	7.50E+15
NA	-43	NA
1.80E+32	0.3	2.30E+16
9.30E+31	-41.1	1.10E+16
1.50E+32	-40.6	1.10E+16
6.20E+32	28	2.60E+16
1.20E+33	165.9	3.70E+16
4.10E+32	45.6	2.30E+16
4.50E+32	-51.8	3.60E+16
2.80E+32	-8	2.10E+16
3.50E+32	-13.2	3.30E+16
1.50E+32	-5.3	2.20E+16
3.70E+32	-60.8	2.20E+16
1.40E+32	13.5	2.00E+16
1.00E+31	-7.5	7.40E+15
3.60E+32	-0.3	2.90E+16
2.40E+33	-232	4.80E+16

Table 7. CME KE, Mass, and Acceleration

Flare Peak Flux	Flare Fluence	Flare Duration	SW h/p
1.19E-04	6.70E-02	20	0.098
2.77E-04	2.10E-01	22	0.082
1.79E-06	NA	NA	0.027
1.33E-06	2.70E-03	39	0.05
5.55E-05	1.20E-03	12	0.116
1.05E-05	4.50E-02	102	0.056
1.71E-05	3.00E-02	44	0.039
1.84E-03	1.50E+00	31	0.098
1.58E-03	6.10E-01	36	0.027
3.16E-06	NA	NA	0.032
9.12E-05	8.60E-02	42	0.037
7.64E-05	3.40E-01	135	0.052
1.66E-04	6.00E-01	115	0.062
5.89E-05	3.30E-02	18	0.062
3.52E-04	4.60E-01	42	0.018
1.37E-04	6.30E-01	120	0.047
9.27E-04	9.10E-01	36	0.191
1.84E-03	2.30E+00	37	0.074
2.03E-05	3.90E-02	53	0.046
2.20E-04	2.00E-01	33	0.069
2.79E-04	1.60E-01	21	0.059
3.86E-04	8.40E-01	188	0.077
7.11E-04	1.30E+00	50	
4.00E-05	6.20E-02	41	0.02
1.30E-04	3.90E-01	73	0.036
3.41E-04	5.10E-01	43	0.032
1.52E-04	1.20E-01	79	0.052
4.47E-06	9.90E-03	53	0.02
2.55E-05	4.40E-02	43	0.054
9.31E-05	5.40E-02	23	0.027
7.00E-04	1.90E-01	20	0.027
8.76E-05	2.00E-01	56	0.025
1.79E-04	3.20E-01	79	0.052
7.97E-05	2.40E-01	73	0.025
5.10E-05	9.90E-02	49	0.018
7.79E-05	3.60E-01	159	0.039
5.05E-05	1.40E-01	60	0.037
1.25E-06	1.10E-02	200	0.022
1.25E-04	2.50E-01	54	0.023
7.31E-05	1.10E-01	49	0.052
1.04E-06	8.60E-04	14	0.014
9.33E-04	NA	NA	0.008
8.28E-04	NA	NA	NA

Table 8. Solar Flare and SEP Parameters

4.2 Linear Fits

Data values for the various solar parameters in this study range from 10^{-4} to 10^{34}. Many of the parameters would be better plotted on logarithmic scales. An examination was made to determine the impact on the CC should logarithmic values be used. Figure 4 shows the CCs of CDAW CME linear speed with 4 MeV A_{He} with linear scaling, semi-log x scaling, semi-log y scaling, and log-log scaling. The h/p values were determined to provide the best results using logarithmic values. Also using logarithmic values are: CME speed, CME mass, CME KE, flare duration, flare flux, and flare fluence. The solar longitude and CME width maintained linear value scaling. Using the linear or logarithmic values as decided on above, linear best fit lines were generated for each pair of parameters being studied. Appendix A contains the linear best fits for each selected CC pairings in this study.

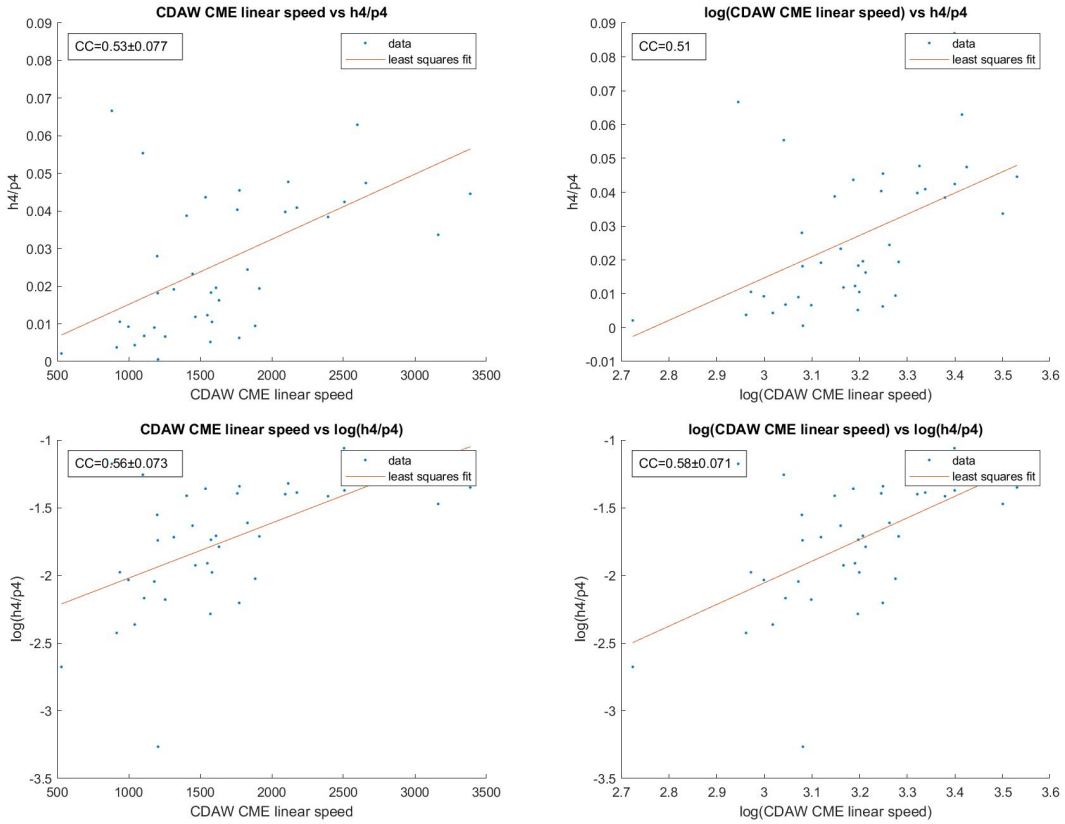

Figure 4. CDAW CME speed correlation plots

4.3 Correlation Coefficients

Correlation coefficients were generated among various SEP, CME, and solar flare parameters. Table 9 is a matrix representation between the various values correlated and the associated correlation coefficient (CC). Boxes highlighted in green have a greater than 99% probability of correlation (highly significant) while boxes highlighted in yellow have been determined to have a greater than 95% probability of correlation (significant). A finer granular breakdown of the CCs will be discussed in the following subsections.

Solar Variable	CC	CC	CC	CC
	log h_4/p_4	log h_8/p_8	log h_{25}/p_{25}	log I_p
West Longitude	-0.05	0.02	-0.06	-0.12
CME width (CDAW)	-0.13	-0.03	0.12	-0.07
CME width (SEEDS)	0.21	0.15	0.31	0.39
Log(CME speed (CDAW))	0.58	0.57	0.51	0.52
Log(CME speed (SEEDS))	0.04	0.29	0.17	0.09
Log(CME KE (CDAW))	0.26	0.22	0.36	0.40
Log(CME acceleration (CDAW))	0.46	0.39	0.18	0.42
Log(CME mass (CDAW))	-0.09	-0.18	0.04	0.16
Log(Flare peak flux)	0.65	0.62	0.56	0.43
Log(Flare fluence)	0.78	0.76	0.66	0.67
Log(Flare duration)	0.11	0.07	0.14	0.38
Log(I_p)	0.72	0.64	0.61	
Log(SW h/p)				0.26

Table 9. Correlation Coefficient Matrix

Solar Wind h/p Correlation Figure 5 shows the least squares fit between solar wind h/p and I_p. The solar wind A_{He} does not significantly correlate with I_p. A caveat is that the margin of error is such that there is the possibility of significant correlation on the error high end. With a Pearson r-value of 0.26 as shown in Table 10, SW A_{He} has a 88% probability of correlating with I_p. This is not statistically significant enough to constitute a confirmed correlation between the two variables. Therefore, there exist a possibility that the SEP does not seed the solar wind and increase the relative He abundances in the solar wind.

	$log(I_p)$
log(SW h/p)	0.26 ± .10

Table 10. Solar Wind h/p & I_p Correlation

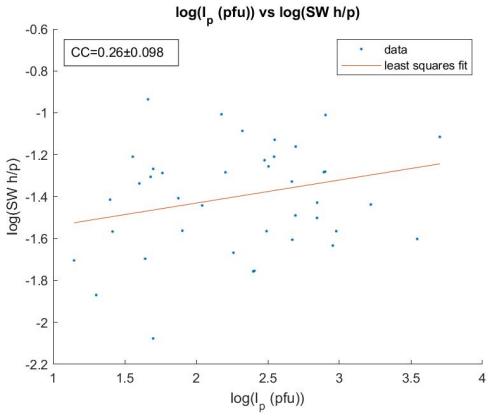

Figure 5. Solar Wind vs SEP Peak Intensity Least-Squares Fit

SEP Peak Intensity Correlation As shown in Figure 6 all three h/p energy values ratios highly significantly correlate with SEP peak intensity. 4 MeV h/p has the largest correlation coefficient with I_p. As the h/p energies increase, the correlation coefficient decreases, but still remains highly significant. This suggest that there exists a possibility that the SEP peak intensity is a potential driver for the higher relative He abundances. The larger intensity during an SEP could be a driver to accelerate the heavier He atoms out of the Corona into space, providing the higher relative abundance.

	$\log(h_4/p_4)$	$\log(h_8/p_8)$	$\log(h_{25}/p_{25})$
$\log(I_p)$	$0.64 \pm .11$	0.07 ± 0.64	0.61 ± 0.07

Table 11. SEP Peak Intensity Correlations

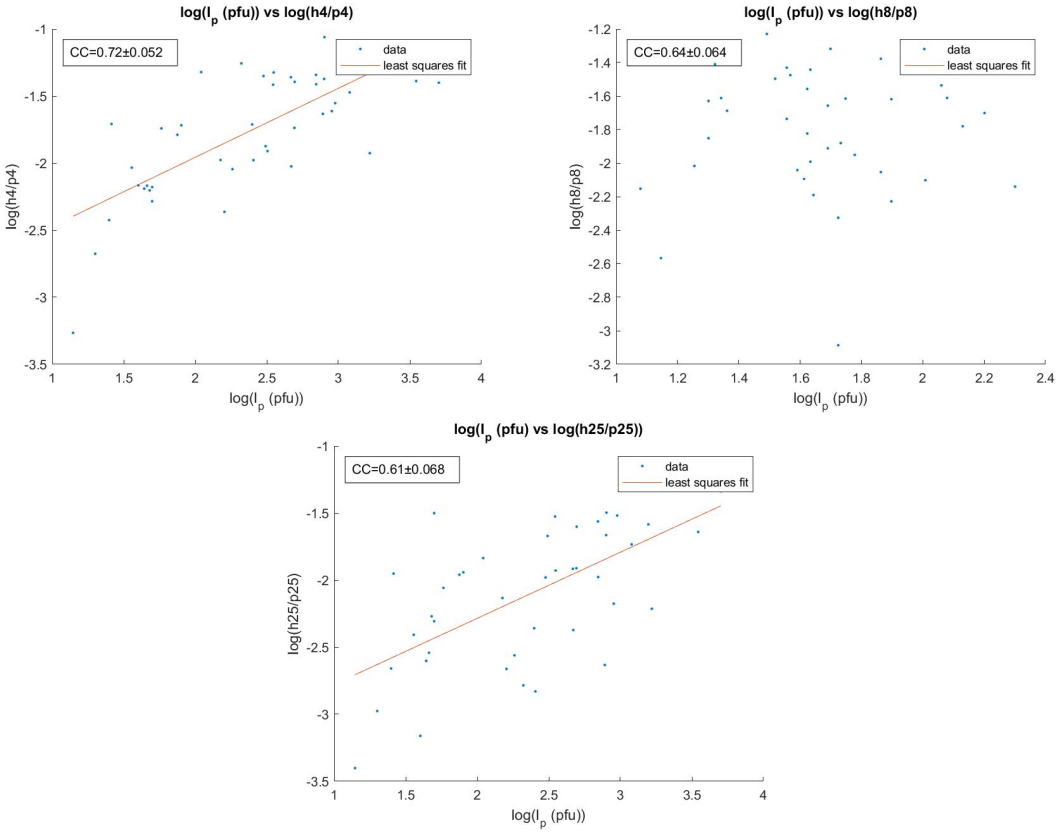

Figure 6. SEP Peak Intensity Least-Squares Fits

Solar West Longitude Correlations Figure 7 shows the least squares fits of solar west longitude with the three h/p ratios and I_p. No correlation exists between the solar west longitude of the event and the various h/p energy ratios not I_p as shown by Table 12. No correlation could potentially show that the increase in relative He abundances is angularly independent with respect to the direction of the SEP. For example, should a greater relative abundance of He be centrally located to direction of the SEP, a correlation should be found. The relative He abundances are equally distributed throughout the SEP.

	$\log(h_4/p_4)$	$\log(h_8/p_8)$	$\log(h_{25}/p_{25})$	$\log\ I_p$
Solar West Longitude	-0.05	0.02	-0.12	-0.12

Table 12. Solar West Longitudes Correlations

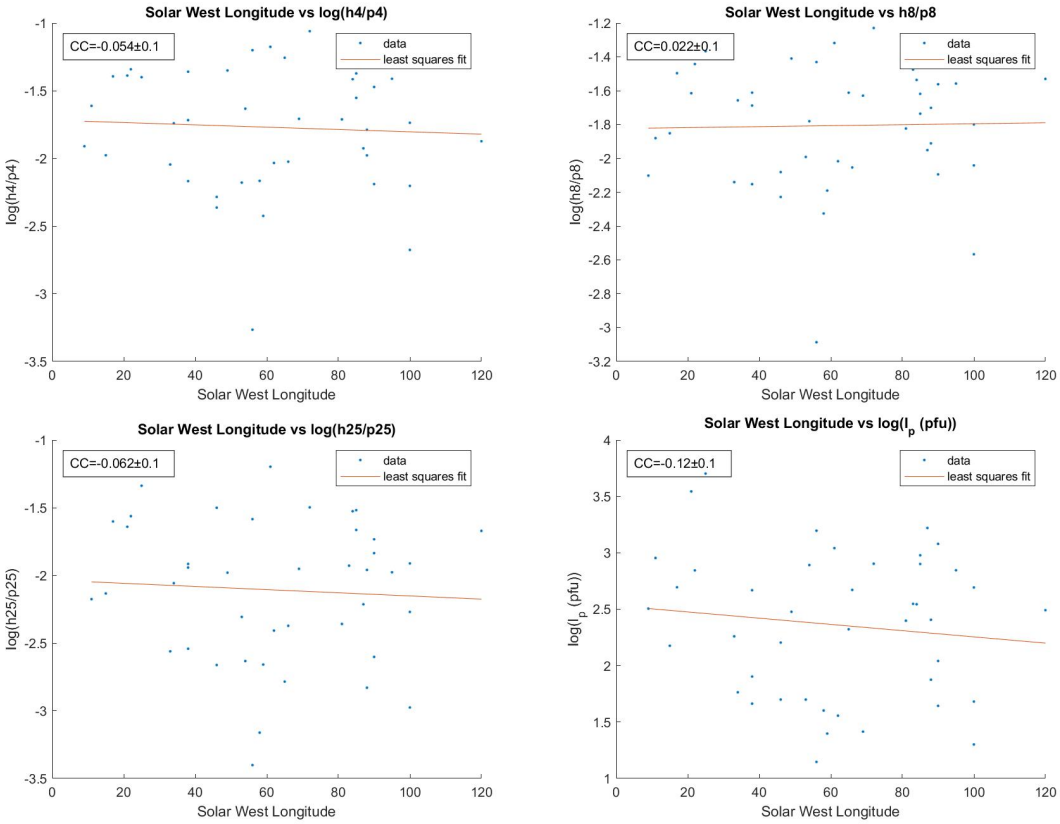

Figure 7. Solar West Longitude Least-Squares Fits

Coronal Mass Ejection Width Correlations Figures 8 and 9 contain the linear fits of variables compared to CME width as measured by CDAW and SEEDS, respectively. As seen in Table 13, the correlation coefficients between CME width and various h/p energy values for the two sensors do not match. This is due to the CME width measurements calculated by CDAW and SEEDS being different. CDAW would frequently return a 360 degree (HALO) CME width as measured by SOHO. CME width as calculated by CDAW does not correlate with the various A_{He} ratios nor does CME width correlate with SEP Peak Intensity (I_p) as shown in table 13.

CME width calculated by SEEDS does not correlate with the 4 or 8 MeV A_{He} ratios. 25 MeV A_{He} does correlate with CME width with greater than a 95% probability. Caution should be noted, however, as the lower bounds on the error in the 25 MeV A_{He} calculation as well as the lower bound of the correlation coefficient are

factored in; 25 Mev A_{He} does not correlate with SEEDS CME width. A lack of highly significant correlation has the potential to show that impulsive and gradual SEPs both do not increase the relative He abundance based on the width of the SEP. A thinner SEP does not increase not decrease the relative abundance of He when compared to a wider SEP.

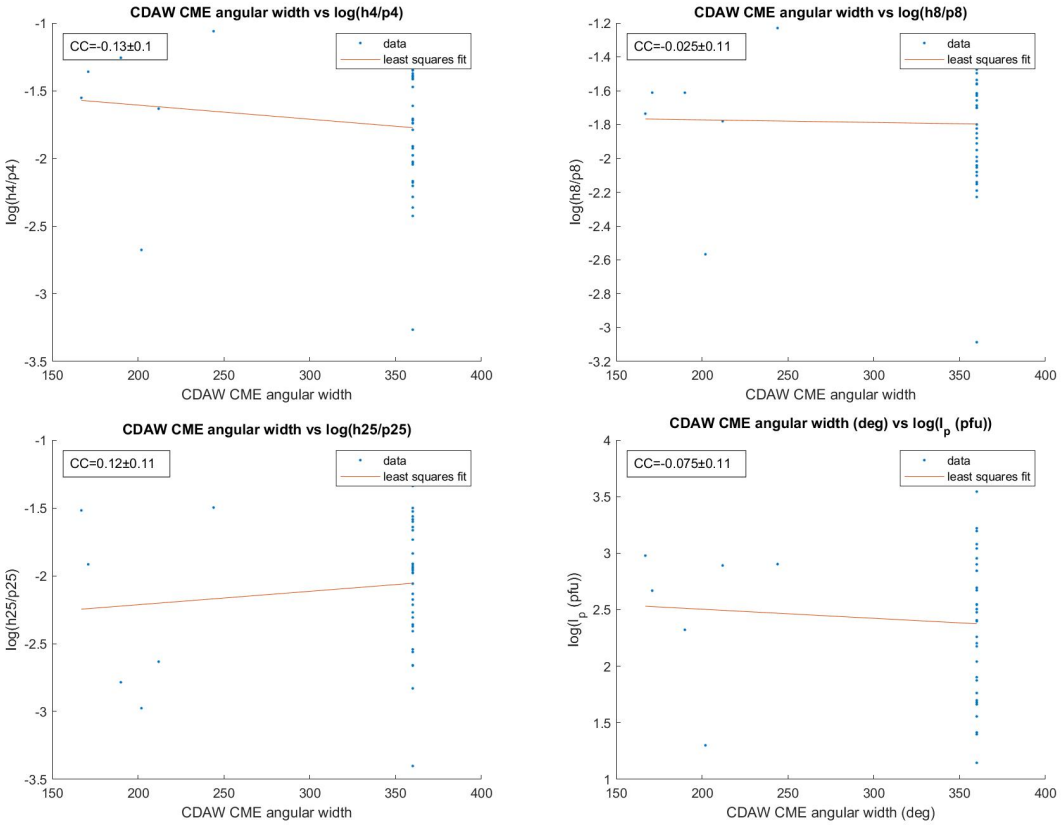

Figure 8. CDAW CME Width Least-Squares Fits

	$\log(h_4/p_4)$	$\log(h_8/p_8)$	$\log(h_{25}/p_{25})$	$\log\ I_p$
CDAW	-0.13 ± .10	-0.03 ± .10	0.12 ± .11	-0.07 ± .11
SEEDS	0.21 ± .10	0.15 ± .10	0.31 ± 0.10	0.39 ± .09

Table 13. CME Width Correlations

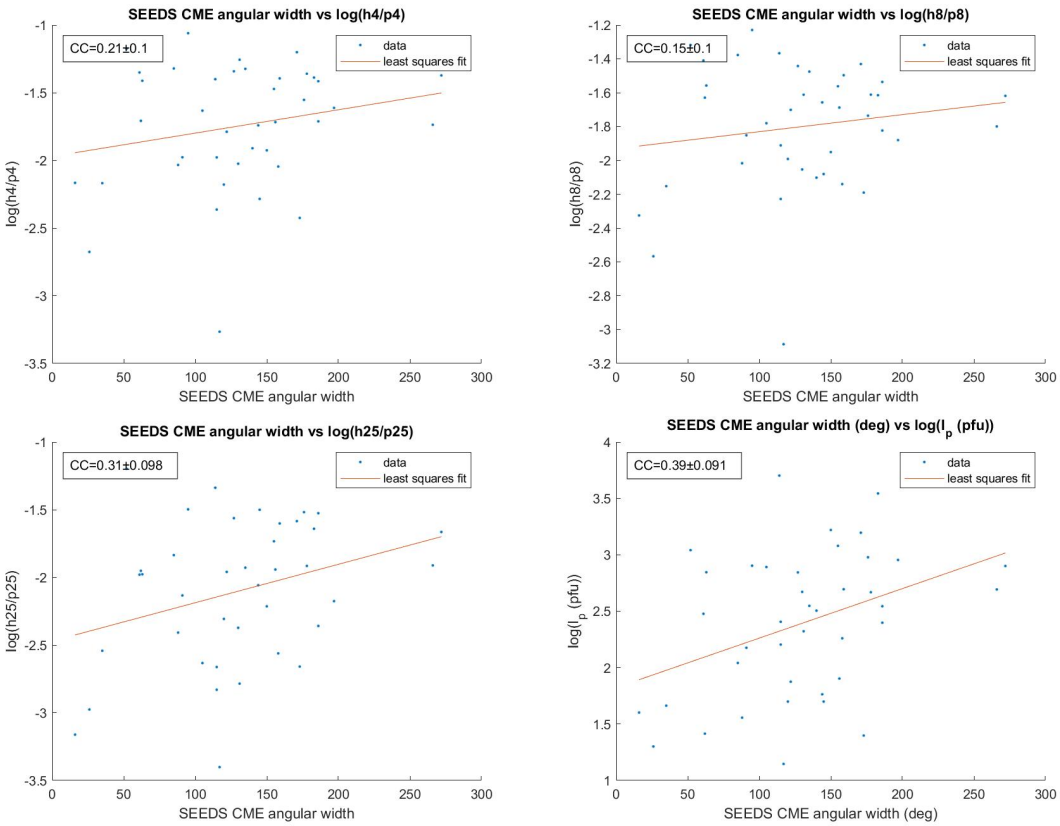

Figure 9. SEEDS CME Width Linear Fits

Coronal Mass Ejection Speed Correlations Tables 10 and 11 show the linear fits of the logarithmic CME speeds for CDAW and SEEDs, respectively. Similarly to CME widths, the correlation coefficients in Table 14 between CME linear speeds and various h/p energy values for the two sensors do not match. Tables 10 and 11 show the linear fits of the logarithmic CME speeds. This is due to how the CME linear speed is calculated by CDAW and SEEDS being different. CDAW uses a linear fit using height-time measurements while SEEDS performs a running-difference image calculation algorithm. CME linear speed as calculated by SEEDS does not correlate with 4, 8, and 25 MeV A_{He} ratios nor does CME linear speed correlate with I_p.

All three energies for A_{He} significantly correlate with CDAW's CME linear speed. Also, I_p significantly correlates with CDAW's CME linear speed. Significant margin for error exists such that the two values will still maintain significant correlation even

at the lower error bounds. The higher CME speeds could be driver for the relative He abundances during a CME. Larger amounts of energy are required in order to increase the speed of the SEP particles. This increase in energy might be what is required to get the heavier He elements to Coronal escape velocity into the. The larger energies responsible for the increased speeds might also ionizing a greater abundance of He atoms. This would allowing more He to be electromagnetically accelerated during a SEP, hence increasing their abundances.

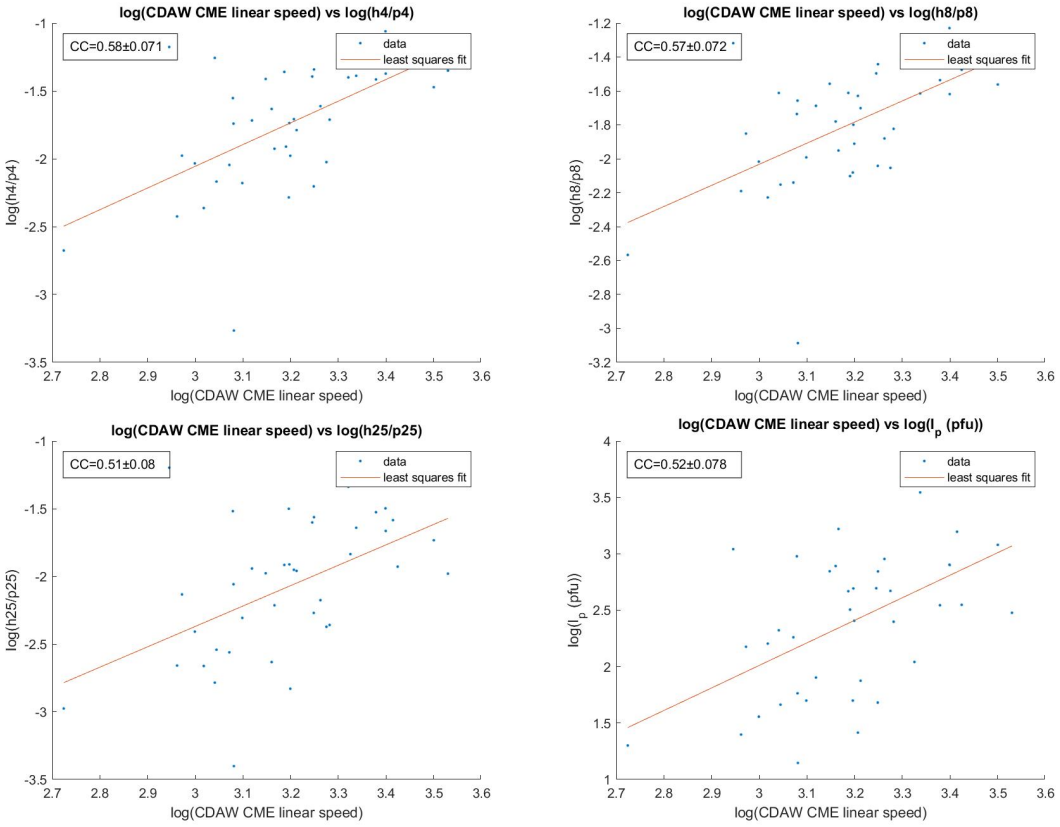

Figure 10. Log(CDAW CME speed) Least-Squares Fits

	$\log(h_4/p_4)$	$\log(h_8/p_8)$	$\log(h_{25}/p_{25})$	$\log\ I_p$
CDAW	$0.58 \pm .07$	$0.57 \pm .07$	$0.51 \pm .08$	$0.52 \pm .08$
SEEDS	$0.04 \pm .11$	$0.29 \pm .11$	0.17 ± 0.10	$0.09 \pm .11$

Table 14. CME Logarithmic Speed Correlations

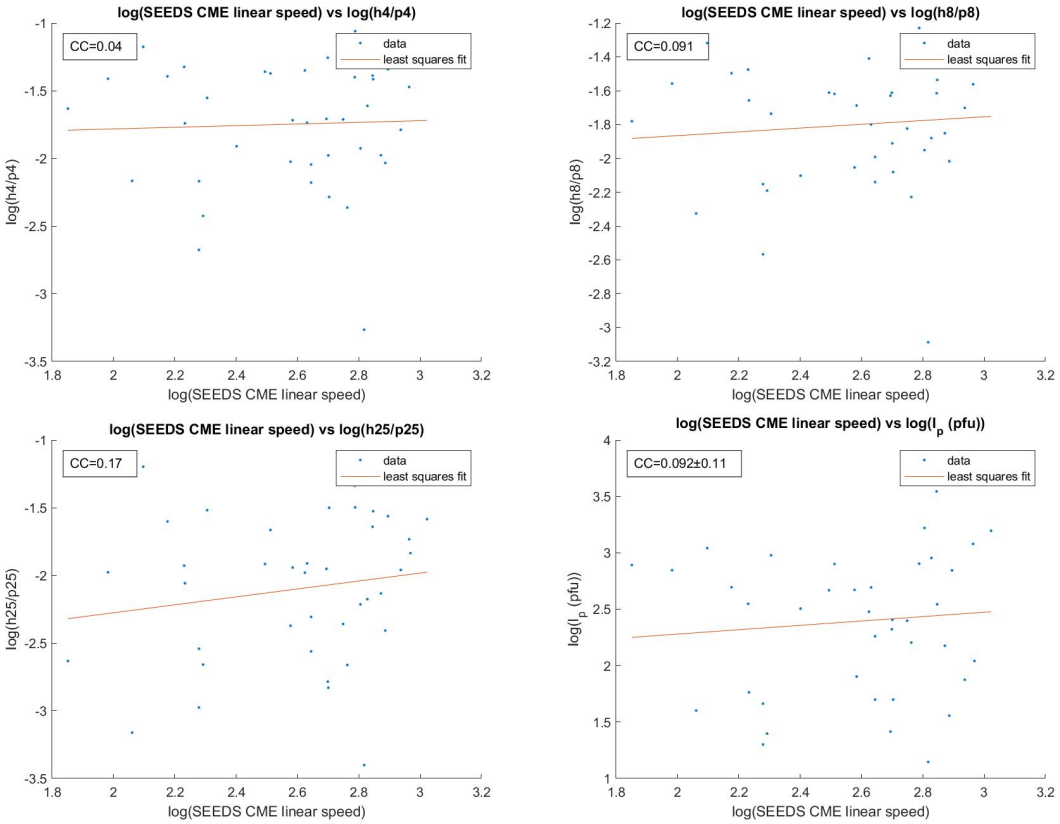

Figure 11. Log(SEEDS CME speed) Least-Squares Fits

Coronal Mass Ejection Kinetic Energy Correlations Upon initial inspection of Figure 12 and Table 15 the CME KE as measured by CDAW does not correlate with the 4 and 8 MeV A_{He}. 25 MeV significantly correlates with CME KE. The error of all three MeV A_{He} CCs is high enough such that there is a potential for all three to significantly correlate, or no correlation to exist. No strong conclusion of the correlation between the CME KE and various A_{He} energies from this study. A lack of KE correlation could potential demonstrate that the energy being used to increase the relative He abundances is not is not mechanical, rather electromagnetic energy.

I_p highly significantly correlates with CME KE. The CC error margin is such that at the worst, I_p significantly correlates with CME KE.

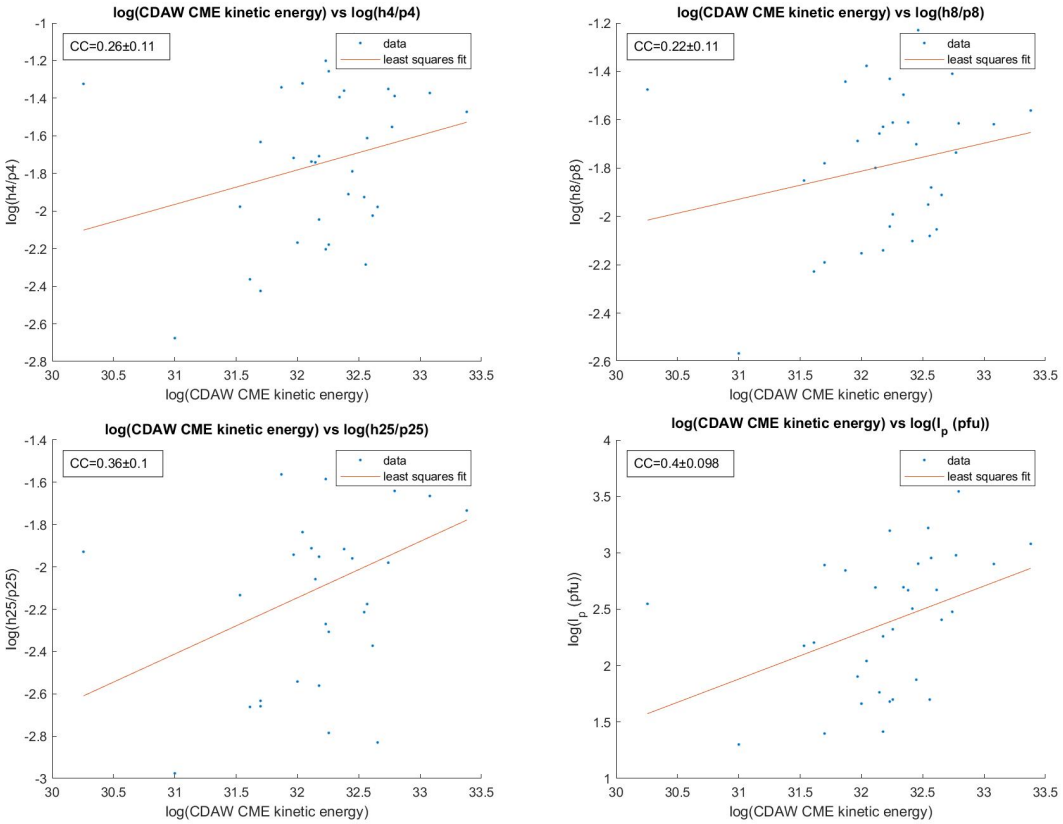

Figure 12. Log(CDAW CME KE) Least-Squares Fits

	$\log(h_4/p_4)$	$\log(h_8/p_8)$	$\log(h_{25}/p_{25})$	$\log\ I_p$
CDAW	0.26 ± 0.11	$0.22 \pm .11$	$0.36 \pm .10)$	$0.40 \pm .10$

Table 15. CME Logrithmic Kinetic Energy Correlations

Coronal Mass Ejection Acceleration Correlations At the lower 4 MeV energies, A_{He} highly significantly correlates with CME acceleration as measured by CDAW as shown in Figure 13 and Table 16. As the energy levels increase to 8 MeV, the correlation with CME acceleration drops to significant. Furthermore, 25 MeV A_{He} does not correlate with CME acceleration. I_p has a highly significant correlation with CME acceleration. There exists a potential that SEP events with a larger CME acceleration could be driving the greater abundance of higher MeV He. Larger electromagnetic forces could be involved to fully ionize the He and provide a greater abundance of $<$ 25 MeV He,

hence why the CME has a larger acceleration. CMEs with weaker acceleration may not be able to provide the electromagnetic forces required to energize He up to <25 MeV at a greater rate than H.

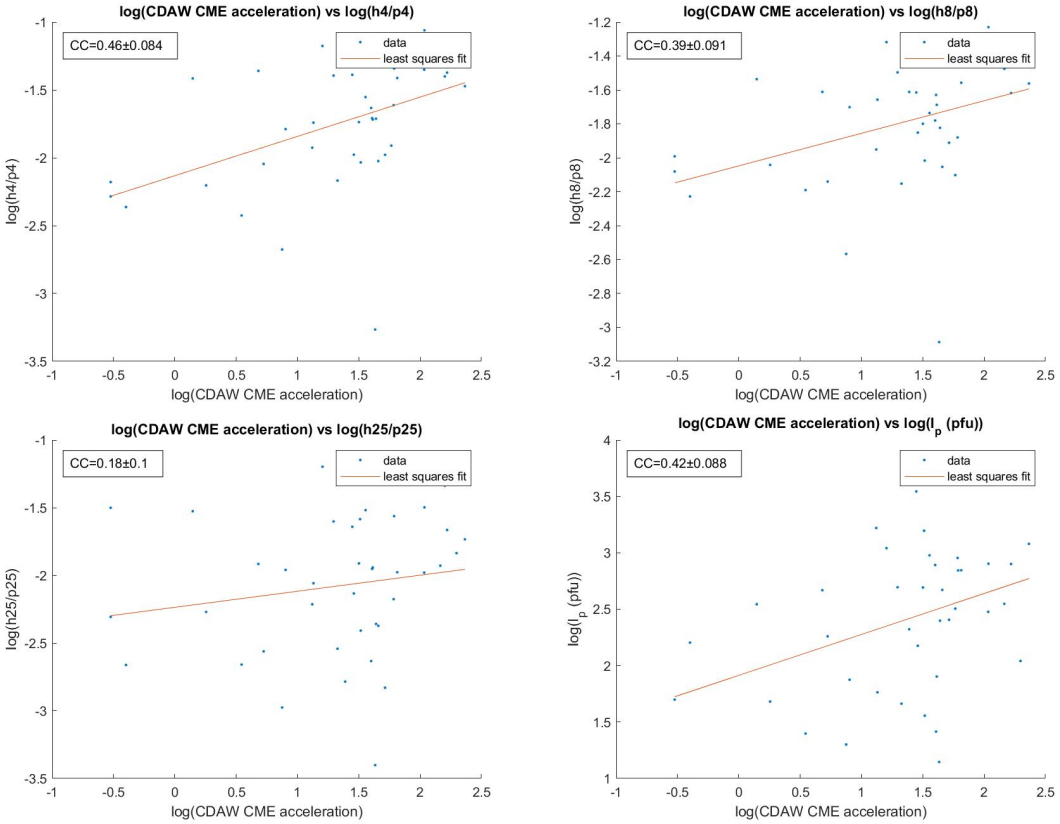

Figure 13. Log(CDAW CME acceleration) Least-Squares Fits

	$\log(h_4/p_4)$	$\log(h_8/p_8)$	$\log(h_{25}/p_{25})$	$\log\ I_p$
CDAW	$0.46 \pm .08$	$0.39 \pm .09$	$0.18 \pm .10$	$0.42 \pm .09$

Table 16. CME Logarithmic Acceleration Correlations

Coronal Mass Ejection Mass Correlations Figure 14 and Table 17 show CME mass does not correlate with the three A_{He} energy values, nor does it correlate with I_p. The lack of correlation suggests that mass expelled from the Sun during an SEP and CME has no factor in increasing the relative He abundances.

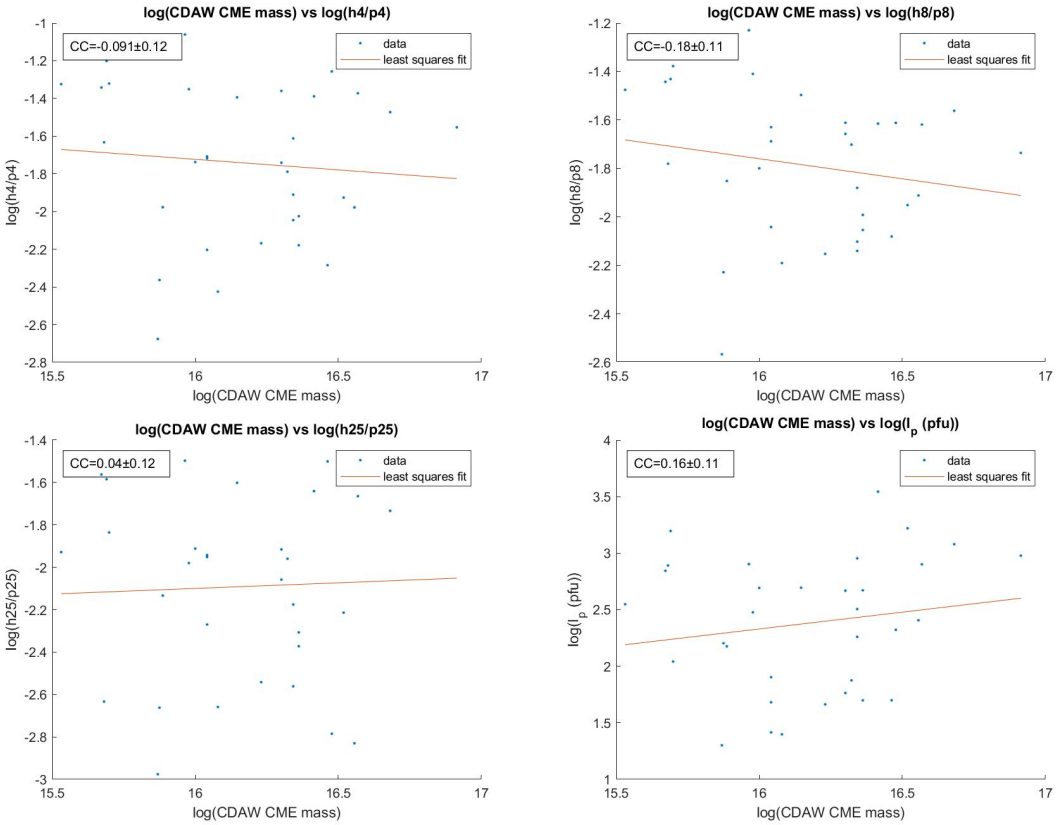

Figure 14. Log(CDAW CME acceleration) Least-Squares Fits

	$\log(h_4/p_4)$	$\log(h_8/p_8)$	$\log(h_{25}/p_{25})$	$\log\ I_p$
CDAW	-0.09 ± .12	-0.18 ± .11	0.04 ± .12	0.16 ± .11

Table 17. CME Logarithmic Mass Correlations

Solar Flare Peak Flux Correlations Solar flare peak flux highly significantly correlates with all three A_{He} energies as shown in Figure 15. There is a slight descending of correlation coefficients as the energy increases as shown in Table 18. There also exists a significant correlation between Solar flare peak flux and I_p. The larger X-ray flux show that greater electromagnetic forces are present at the source of the SEP. The larger electromagnetic forces a the flare location could be the driving mechanism for the increased relative He abundances as a greater number of He atoms can be ionized and accelerated to greater energies by the flare.

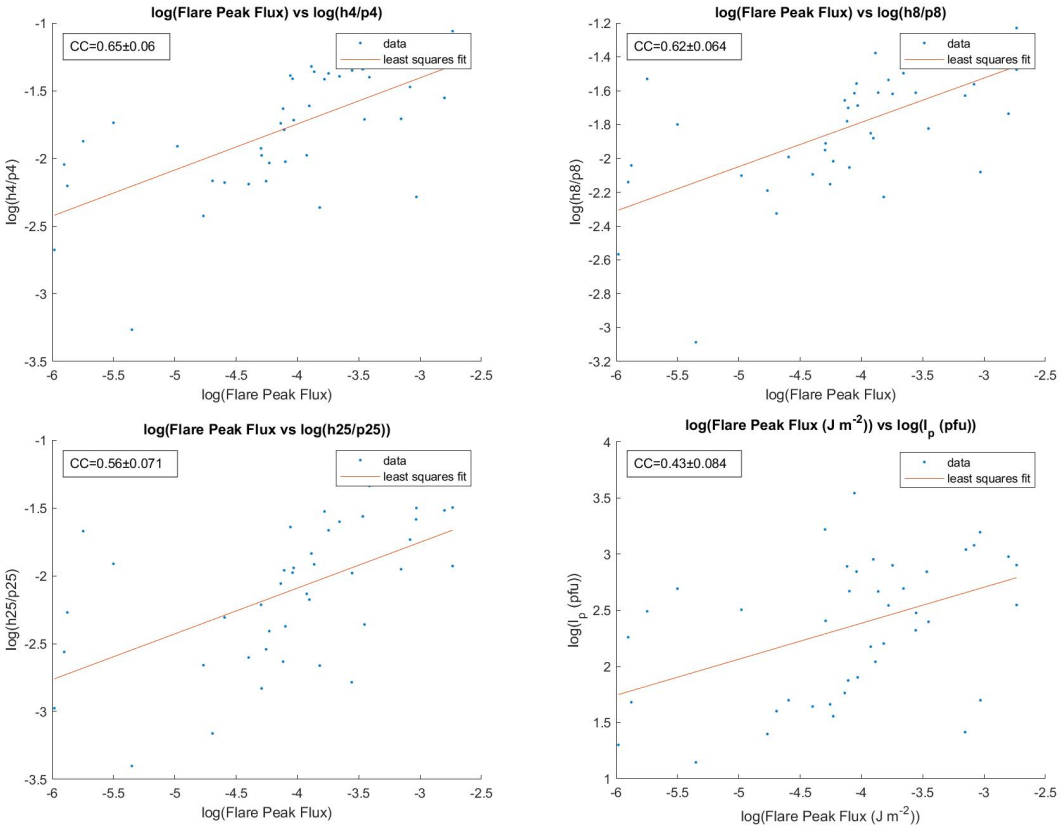

Figure 15. Log(Flare Peak Flux) Least-Squares Fits

$\log(h_4/p_4)$	$\log(h_8/p_8)$	$\log(h_{25}/p_{25})$	$\log\ I_p$
0.65 ± .06	0.62 ± .06	0.56 ± .07	0.43 ± .08

Table 18. Solar Flare Logarithmic Peak Flux Correlations

Solar Flare Fluence Correlations Similar to Solar flare peak flux, Figure 16 shows solar flare fluence significantly correlates with all three A_{He} energies. The correlation coefficients also decrease as the energies increase. Of all parameters correlated in this study, the solar flare fluence has the strongest correlation with the A_{He} energies as shown in Table 19. The solar flare fluence highly significantly correlates with I_p. Similarly to solar flare flux, a larger solar flare fluence show a greater amount of energy being generated at the solar flare site. The larger solar flare energy could be producing a greater abundance of He with respect to H ions.

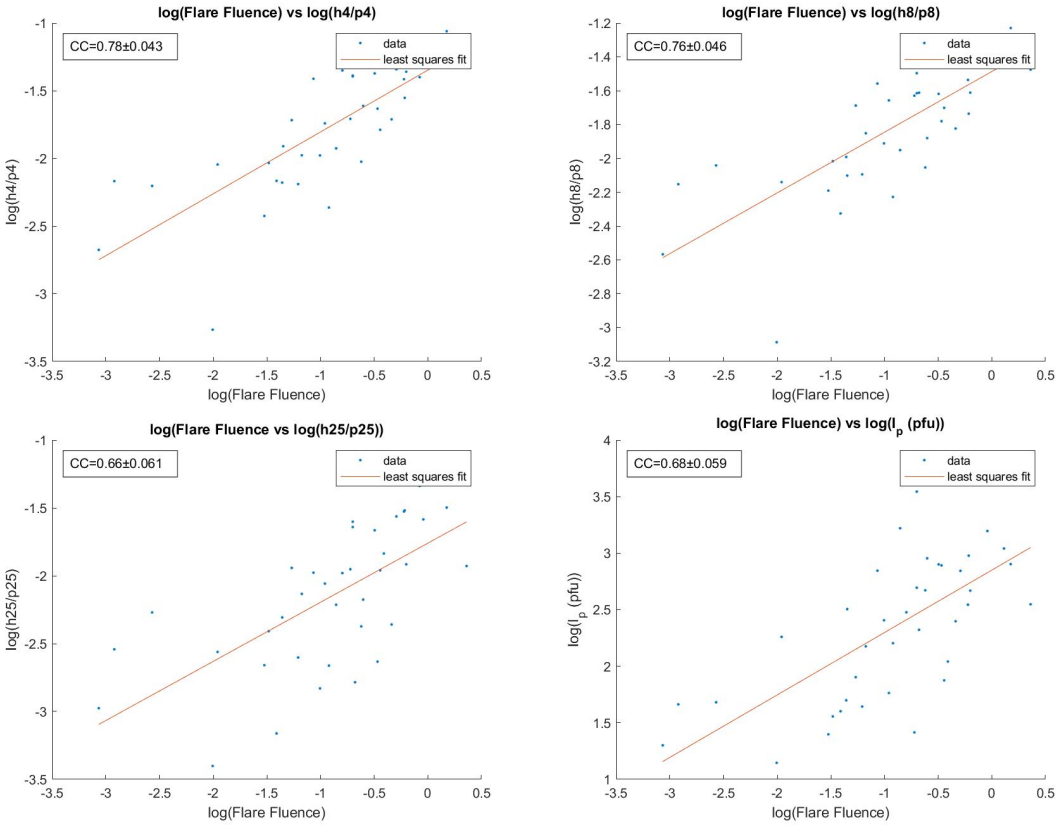

Figure 16. Log(Flare Peak Fluence) Least-Squares Fits

$\log(h_4/p_4)$	$\log(h_8/p_8)$	$\log(h_{25}/p_{25})$	$\log\ I_p$
0.78 ± .04	0.76 ± .05	0.66 ± .06	0.67 ± .06

Table 19. Solar Flare Logarithmic Fluence Correlations

Solar Flare Duration Correlations Figure 17 demonstrates that no correlation exists between the solar flare duration and the 4, 8, and 25 MeV A_{He}. A significant correlation exists between solar flare duration and I_p. The lack of correlation with solar flare duration could show that the increase relative abundance is not reliant on how long the solar flare is occurring. A greater duration solar flare does not produce a greater relative abundance of He ions with energies above 4 MeV.

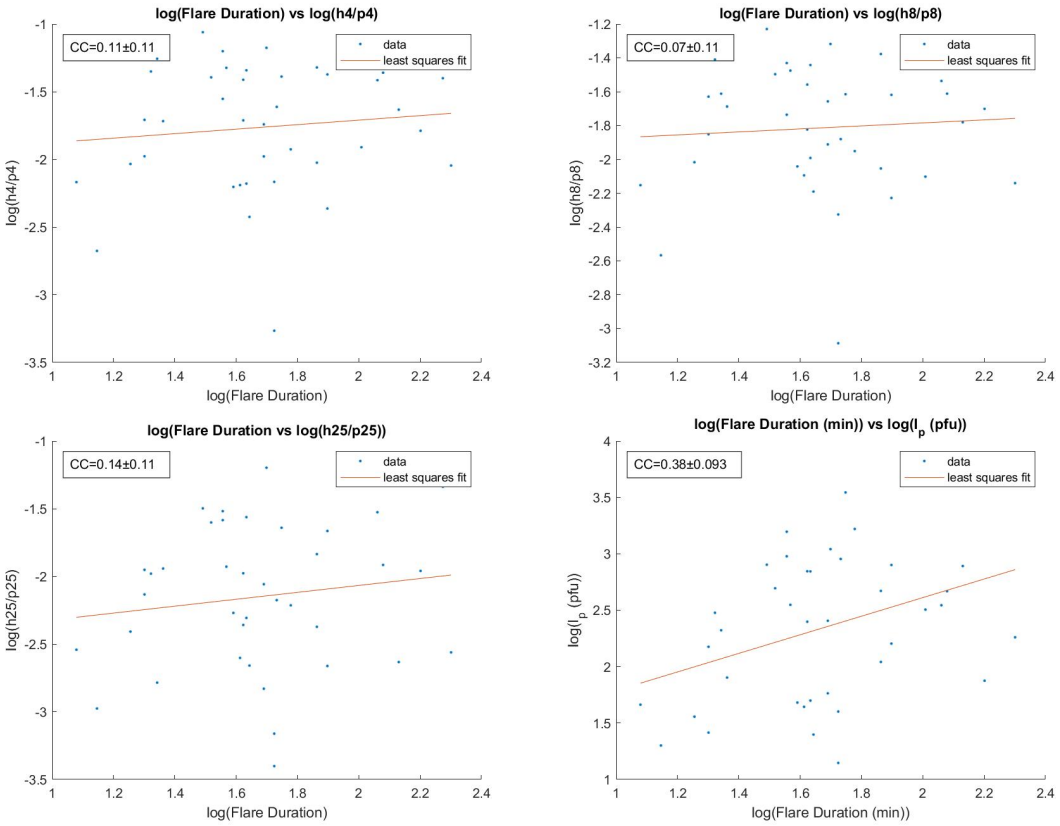

Figure 17. Log(Flare Duration) Least-Squares Fits

$\log(h_4/p_4)$	$\log(h_8/p_8)$	$\log(h_{25}/p_{25})$	$\log I_p$
$0.11 \pm .11$	$0.07 \pm .07$	$0.11 \pm .14$	$0.38 \pm .09$

Table 20. Solar Flare Logarithmic Duration Correlations

V. Conclusion

5.1 Non-correlating Parameters

This study found many parameters that did not correlate. Table 21 contains the parameters that showed no correlation with the three A_{He} ratios. Also found is this study was a lack of correlation between SEP peak intensity and the solar wind h/p ratio.

	$\log(h_4/p_4)$	$\log(h_8/p_8)$	$\log(h_{25}/p_{25})$
Solar Longitude	No significance	No significance	No significance
CDAW CME Width	No significance	No significance	No significance
SEEDS CME Width	No significance	No significance	No significance
log(SEEDS CME Speed)	No significance	No significance	No significance
log(CME KE)	No significance	No significance	No significance
log(CME Mass)	No significance	No significance	No significance
log(Solar Flare Duration)	No significance	No significance	No significance

Table 21. Non-Correlating Paramters

The lack of correlation between the $< 4MeV$ h/p ratios and the parameters in Table 21 will assist in ruling out different causes as to the relative He abundance increase during SEPs. For example, Kahler & Brown (2021) made the assumption that the SW A_{He} is independent of SEP peak intensive. The lack of significant correlation found in this study between those two parameters lends weight to support Kahler & Brown's assumption. This also lends weight to Kahler & Brown's conclusion of some connection between the SW and SEP h/p ratios.

5.2 Correlating Parameters

Also found in this study were multiple parameters with highly significant correlation. These parameters are displayed in Table 22.

	$\log(h_4/p_4)$	$\log(h_8/p_8)$	$\log(h_{25}/p_{25})$
log(SEP Peak Intensity)	High Significance	High Significance	High Significance
log(CDAW CME linear speed)	High Significance	High Significance	High Significance
log(Flare Peak Flux)	High Significance	High Significance	High Significance
log(Flare Fluence)	High Significance	High Significance	High Significance

Table 22. Correlating Parameters

The highly significant correlation between the three higher energy A_{He} ratios and the solar flare peak flux and duration lends to a potential causal link of solar flares playing a role in the relative He abundance increase over the SW. The correlating parameters are all parameters that are cause by an increase of electromagnetic energy at the Sun. The increase in energy could be ionizing a greater relative number of He atoms. This would allow a greater abundance of He ions to be susceptible to the electromagnetic forces at the event site. These He ions would then be able to be expelled by the CME, hence potentially causing the greater relative abundance at the Earth.

With a slight lower CC than solar flares, a highly significant correlation between the three A_{He} ratios and the CME linear speed could potentially shed light into the CME speed's roll in increasing the relative He ratios. The higher speeds demonstrate larger energies are present at the CME ejection site.

Of significant note is the correlation between the three h/p energy ratios and CDAW CME acceleration. A highly significant correlation was found with the acceleration and the lower 4 MeV ratios, a significant correlation with the 8 MeV h/p ratio, and no correlation with the 25 MeV h/p ratio. The larger CME accelerations could play a part in increasing lower energy He abundance ratios.

5.3 Further Study

The highly significant correlations will give weight to theories on elemental abundance enhancements during solar events. Investigation onto the mechanisms that generate the relative He abundance during SEP can be performed. Also, investigation into the trend of increasing correlation between h/p and CME acceleration can be performed on energies <4 MeV. The CME linear speed from the SEEDS catalog did not correlate with A_{He} ratios, but the CDAW linear speeds significantly correlated with A_{He} ratios. Further investigation should be done into the SEEDS linear speed calculations as to the cause for this error.

5.4 Conclusion

The highly significant correlations will give weight to theories on elemental abundance enhancements during SEP events. Solar flares significantly correlate with relative He abundance increases during CMEs. A causal link is most likely existent. Potential causal as well in the CME linear speed. Different solar events are inevitably linked and this study shed light on potential causal links to be further investigated.

Bibliography

Brodrick, D., Tingay, S., and Wieringa, M. (2005). X-ray magnitude of the 4 november 2003 solar flare inferred from the ionospheric attenuation of the galactic radio background. *Journal of Geophysical Research: Space Physics*, 110(A9).

Desai, M., Mason, G., Dayeh, M., Ebert, R., Mccomas, D., Li, G., Cohen, C., Mewaldt, R., Schwadron, N., and Smith, C. (2016). Spectral properties of large gradual solar energetic particle events I. Fe, O, and seed material. *The Astrophysical Journal*, 816(2):68.

Dierckxsens, M., Tziotziou, K., Dalla, S., Patsou, I., Marsh, M., Crosby, N., Malandraki, O., and Tsiropoula, G. (2015). Relationship between solar energetic particles and properties of flares and cmes: statistical analysis of solar cycle 23 events. *Solar Physics*, 290(3):841–874.

DoD (2018). *Joint Publication 3-14, Space Operations*. Department of Defense.

Drake, J. F., Cassak, P., Shay, M., Swisdak, M., and Quataert, E. (2009). A magnetic reconnection mechanism for ion acceleration and abundance enhancements in impulsive flares. *The Astrophysical Journal Letters*, 700(1):L16.

Eells, W. C. (1929). Formulas for probable errors of coefficients of correlation. *Journal of the American Statistical Association*, 24(166):170–173.

Frazier, S. (2016). Nasa: Understanding the magnetic sun. `https://www.nasa.gov/feature/goddard/2016/understanding-the-magnetic-sun`. [Online; accessed 25-April-2021].

Kahler, S. and Brown, D. (2021). Variations of peak He/H ratios in solar energetic

(E > 4 MeV) particle events and comparisons with solar wind He/H ratios. *The Astrophysical Journal*, 908(2):214.

Kahler, S. and Ling, A. (2019). Suprathermal ion backgrounds of solar energetic particle events. *The Astrophysical Journal*, 872(1):89.

Parker, E. N. (1958). Dynamics of the interplanetary gas and magnetic fields. *The Astrophysical Journal*, 128:664.

Pisacane, V. L. (2008). *The space environment and its effects on space systems*. American Institute of aeronautics and Astronautics.

Reames, D. V. (2016). The origin of element abundance variations in solar energetic particles. *Solar Physics*, 291(7):2099–2115.

Reames, D. V. (2018). Abundances, ionization states, temperatures, and fip in solar energetic particles. *Space Science Reviews*, 214(3):61.

Reames, D. V. (2020). Four distinct pathways to the element abundances in solar energetic particles. *Space Science Reviews*, 216(2):1–29.

Round, J., Loper, R., Nava, O., and Kahler, S. (2016). Variations of h-normalized heavy-ion abundances in large solar energetic (E > 10 MeV) particle events.

Round, J. F. (2019). Variations of heavy ion abundances relative to proton abundances in large solar energetic particle events.

Taylor, J. (1997). *Introduction to error analysis, the study of uncertainties in physical measurements*.

Trottet, G., Samwel, S., Klein, K.-L., De Wit, T. D., and Miteva, R. (2015). Statistical evidence for contributions of flares and coronal mass ejections to major solar energetic particle events. *Solar Physics*, 290(3):819–839.

Zell, H. (2015). The heliospheric current sheet. https://www.nasa.gov/content/goddard/heliospheric-current-sheet. [Online; accessed 01-Aug-2021].

REPORT DOCUMENTATION PAGE

Form Approved
OMB No. 0704–0188

1. REPORT DATE *(DD–MM–YYYY)*	2. REPORT TYPE	3. DATES COVERED *(From — To)*
19–08–2021	Master's Thesis	May 2019 — Sep 2021

4. TITLE AND SUBTITLE

RELATIONSHIP BETWEEN SOLAR ENERGETIC PARTICLE HE/H ABUNDANCE RATIOS AND PROPERTIES OF FLARES AND CMES

5a. CONTRACT NUMBER

5b. GRANT NUMBER

5c. PROGRAM ELEMENT NUMBER

6. AUTHOR(S)

Christopher R. Davidson, Capt, USAF

5d. PROJECT NUMBER

5e. TASK NUMBER

5f. WORK UNIT NUMBER

7. PERFORMING ORGANIZATION NAME(S) AND ADDRESS(ES)

Air Force Institute of Technology
Graduate School of Engineering and Management (AFIT/EN)
2950 Hobson Way
WPAFB OH 45433-7765

8. PERFORMING ORGANIZATION REPORT NUMBER

AFIT-ENP-MS-21-S-025

9. SPONSORING / MONITORING AGENCY NAME(S) AND ADDRESS(ES)

Air Force Research Laboratory/Space Vehicles
3550 Aberdeen Avenue SE
Kirtland AFB, NM 87117
DSN 263-3517, COMM 505-853-3517
Email: stephen.kahler@us.af.mil

10. SPONSOR/MONITOR'S ACRONYM(S)

AFRL/RV

11. SPONSOR/MONITOR'S REPORT NUMBER(S)

12. DISTRIBUTION / AVAILABILITY STATEMENT

DISTRIBUTION STATEMENT A:
APPROVED FOR PUBLIC RELEASE; DISTRIBUTION UNLIMITED.

13. SUPPLEMENTARY NOTES

14. ABSTRACT

Previous studies have investigated the He/H elemental abundance ratios of Solar Energetic Particle (SEP) Events of energies above 4 MeV. Also, studies have investigated the correlations between SEPs, Coronal Mass Ejections (CME), and Solar Flares. This work finds the correlations between the >4 MeV He/H abundance ratios and the solar parameters from the SEP, CME, and solar flare associated with the abundance increases. 43 SEP events located at solar west longitude are analyzed to find the correlation coefficients. Highly significant correlation was found between the He/H abundance ratios and the following parameters: solar flare flux, solar flare fluence, CME linear speed, and SEP peak intensity. No correlation was found between the He/H abundance ratios and the following parameters: solar longitude, CME width, CME mass, and solar flare duration.

15. SUBJECT TERMS

Elemental Abundances, Solar Energetic Particles, Coronal Mass Ejections. Solar Flares

16. SECURITY CLASSIFICATION OF:			17. LIMITATION OF ABSTRACT	18. NUMBER OF PAGES	19a. NAME OF RESPONSIBLE PERSON
a. REPORT	b. ABSTRACT	c. THIS PAGE			Maj Daniel J. Emmons, AFIT/ENP
U	U	U	U	58	19b. TELEPHONE NUMBER *(include area code)* (937) 255-3636, x4571; Daniel.Emmons@afit.edu